Food Research International 245 (2026) 120837

Contents lists available at ScienceDirect

Food Research International

journal homepage: www.elsevier.com/locate/foodres

A multi-platform characterization reveals the biochemical and sensory evolution of Pancetta Piacentina PDO throughout 240 days of ripening

Gabriele Rocchetti [a,*], Federico Froldi [a], Giulia Fappani [a], Michela Errico [a], Maria Chiara Fontanella [b], Samantha Sigolo [a], Alessandra Scansani [c], Aldo Prandini [a]

[a] Department of Animal Science, Food and Nutrition, Università Cattolica del Sacro Cuore, Via Emilia Parmense 84, 29122 Piacenza, Italy
[b] Department for Sustainable Food Process, Università Cattolica del Sacro Cuore, Via Emilia Parmense 84, 29122 Piacenza, Italy
[c] Consorzio Tutela Salumi DOP Piacentini, Via Tirotti 11, 29122 Piacenza, Italy

ARTICLE INFO

Keywords:
Dry-cured meat
UHPLC-HRMS
Redox markers
Data fusion
Omics technologies

ABSTRACT

Pancetta Piacentina Protected Designation of Origin is a traditional Italian dry-cured meat product whose quality is shaped by complex biochemical changes during ripening, yet the molecular evolution underlying quality development remains poorly understood. This study provided a multi-platform characterization of Pancetta Piacentina ripening by combining fatty acid profiling, redox marker evaluation, untargeted metabolomics, lipidomics, volatile profiling, and sensory analysis. Ripening was characterized by progressive dehydration, a reduction in the relative proportion of polyunsaturated fatty acids, and changes in lipid oxidation, as indicated by variations in peroxide value and thiobarbituric acid reactive substances together with marked reduction of the endogenous glutathione system. Metabolomics revealed extensive metabolic remodeling associated with proteolysis and lipid-related transformations, whereas lipidomics highlighted relative reduction of glycerophospholipids and changes in fatty acyls, glycerolipids, and sphingolipids. Volatile profiling and sensory analysis provided complementary evidence of the development of characteristic aroma and sensory attributes during maturation. Finally, supervised DIABLO analysis integrating the metabolomics and lipidomics datasets identified model-derived associations between selected molecular features contributing to the discrimination of ripening stages. Overall, the complementary analytical layers provide a comprehensive view of the biochemical and sensory evolution of Pancetta Piacentina PDO throughout ripening.

1. Introduction

"Pancetta Piacentina" is a traditional Italian dry-cured meat product granted Protected Designation of Origin (PDO) status under Commission Regulation (EC) No 1263/96. It is produced from pork belly of heavy pigs according to the official PDO production specifications, involving dry-salting with salt and natural spices, rolling, tying, and ripening under controlled temperature and relative humidity for at least four months. During ripening, dehydration, proteolysis, lipolysis, and oxidative reactions collectively contribute to the physicochemical, biochemical, and sensory characteristics of the final product (Domínguez, Pateiro, et al., 2019; Petrova et al., 2015).

Lipid metabolism plays a central role in these transformations. Lipolysis releases free fatty acids that act as precursors of volatile and non-volatile compounds contributing to aroma development (Jin et al., 2010), while also providing substrates for oxidative reactions, as reported for Coppa Piacentina PDO (Leni et al., 2024). Lipid oxidation is therefore a key determinant of dry-cured meat quality, contributing to desirable flavor development but potentially causing detrimental effects on sensory properties and nutritional value when excessive (Domínguez, Pateiro, et al., 2019). Belly-derived products such as Pancetta are particularly prone to oxidation because of their high fat content (Pleadin et al., 2021). In other PDO meat products, ripening has been associated with reduction in the relative proportion of PUFA and accumulation of lipid oxidation products (Rocchetti et al., 2025), highlighting the value of combining fatty acid profiling with oxidative markers. Peroxide value and thiobarbituric acid reactive substances (TBARS) are widely used to monitor lipid oxidation, while the glutathione system provides complementary information on redox status (Domínguez, Pateiro, et al., 2019). Ripening also induces moisture loss and changes in protein, lipid, and ash contents, with NaCl playing an important role in modulating water activity, protein stability, and oxidative processes

* Corresponding author.
E-mail address: gabriele.rocchetti@unicatt.it (G. Rocchetti).

https://doi.org/10.1016/j.foodres.2026.120837
Received 9 August 2026; Received in revised form 11 September 2026; Accepted 14 September 2026
Available online 16 September 2026
0963-9969/© 2026 The Authors. Published by Elsevier Ltd. This is an open access article under the CC BY-NC-ND license (http://creativecommons.org/licenses/by-nc-nd/4.0/).

(Domínguez, Pateiro, et al., 2019; Rocchetti et al., 2023; Ruiz-Ramírez et al., 2005).

Recent advances in omics technologies have expanded the molecular characterization of dry-cured meat products. Untargeted metabolomics has been used to investigate metabolic changes associated with proteolysis, microbial activity, and ripening, whereas lipidomics has provided insights into lipid remodeling and oxidative processes during curing and processing (Caballero et al., 2025; Fu et al., 2025; Mediani et al., 2022; Rocchetti et al., 2025; Rutigliano et al., 2023). Nevertheless, integrated metabolomics-lipidomics investigations of PDO dry-cured meats remain limited, particularly for Pancetta Piacentina PDO. Existing studies on this product have mainly addressed specific aspects such as microbial characterization (Busconi et al., 2014), while the molecular mechanisms underlying ripening and their relationship with sensory and aroma development remain poorly characterized. Multivariate data fusion of complementary omics datasets can provide a comprehensive description of coordinated molecular changes in complex food matrices (Tomas et al., 2024).

Therefore, this study aimed to comprehensively characterize the ripening of Pancetta Piacentina PDO through a multi-platform analytical approach combining conventional compositional analyses, fatty acid profiling, redox markers, untargeted metabolomics, lipidomics, volatile profiling, and sensory analysis. Formal multivariate integration was further applied to the metabolomics and lipidomics datasets using DIABLO to identify molecular features contributing to the discrimination of ripening stages. Volatile profiling and sensory analysis were used as complementary analytical approaches to further contextualize the biochemical changes associated with maturation and the development of product quality.

2. Materials and methods

2.1. Collection of Pancetta Piacentina PDO samples

Pancetta Piacentina PDO samples were provided by Salumificio Giordano (Carpaneto Piacentino, Piacenza, Italy), a producer belonging to the "Salumi Piacentini PDO Consortium". The study included six individual biological samples at each predefined ripening stage: 0 (T0, fresh, untreated pork belly), 60 (T60), 120 (T120), 180 (T180), and 240 (T240) days, for a total of 30 samples. Each biological replicate represented an independent Pancetta obtained from a different animal, and samples collected at the different ripening stages originated from different production batches. Thus, the 30 samples represented independent biological units, and sampling was destructive rather than repeated on the same product over time. Accordingly, the individual Pancetta sample was considered the experimental unit. The pork bellies were supplied by Martelli F.lli S.p.A. (Dosolo, Italy) and originated from pigs of the same genetic type bred on a single farm and slaughtered at the same slaughterhouse. The bellies used for the study had comparable initial weight and size and were processed and ripened at the same salami factory according to the official Pancetta Piacentina PDO product specification. According to the PDO specification, processing starts with dry salting using a mixture containing sodium chloride (1.5–3.5 kg/100 kg fresh meat), sodium and/or potassium nitrate ($\leq$ 15 g/100 kg), black and/or white pepper (30–50 g/100 kg), cloves ($\leq$ 40 g/100 kg), sugars ($\leq$ 1.5 kg/100 kg), and sodium L-ascorbate ($\leq$ 200 g/100 kg). Salting is performed manually, followed by storage at 3–5 °C and 70–90% relative humidity for at least 10 days. After salting and trimming, the Pancette are rolled, tied, perforated, and subjected to a short resting phase at 0–5 °C, followed by a drying phase of up to 7 days at 15–25 °C. The subsequent ripening phase lasts for at least four months from salting and is conducted at 10–14 °C and 70–90% relative humidity. T0 samples were collected in April 2025 from fresh, untreated pork bellies before the application of any technological treatment, including salting, spice addition, and ripening. Samples at the subsequent ripening stages were collected at the predefined time points throughout the production cycle, with the final T240 sampling performed in November 2025. At each stage, a central portion was collected from each individual sample and divided into two approximately equal subsamples, which were vacuum-packed. One subsample was used for sensory analysis, whereas the other was transported to the Università Cattolica del Sacro Cuore (Piacenza, Italy) for chemical analyses. Before chemical analyses, the covering rind was removed and samples were completely minced using a meat grinder (Bosch MFW68660, Robert Bosch GmbH, München, Germany), followed by manual kneading to ensure sample homogeneity. Aliquots for untargeted metabolomics and lipidomics were immediately stored at −80 °C. All omics analyses were performed after completion of the sampling campaign, with samples from all ripening stages analyzed within a single analytical batch to minimize analytical batch effects.

2.2. Proximate composition and mineral analysis

Proximate composition was determined according to ISO methods for moisture (ISO, 1997), ether extract (ISO, 1973), and ash (ISO, 1998), and according to AOAC method 984.13 (AOAC, 2000) for crude protein. For mineral analysis, samples were frozen and lyophilised at −50 °C. Approximately 0.5 g of lyophilised sample was digested with 5 mL of 65% HNO_3 using a microwave digestion system (Mars 5 Express, CEM, USA) at 1600 W, with sequential steps of 5, 5, and 10 min at 100, 150, and 200 °C, respectively. After cooling, digests were diluted to 50 mL with ultrapure water and filtered through 0.45 μm nylon membranes. Sodium (Na), copper (Cu), iron (Fe), and zinc (Zn) were quantified by inductively coupled plasma optical emission spectrometry (ICP-OES 5100, Agilent Technologies, Santa Clara, CA, USA), using the operating conditions reported in Supplementary Table 1, whereas selenium (Se) was determined by inductively coupled plasma mass spectrometry (ICP-MS 7800, Agilent Technologies), using the conditions reported in Supplementary Table 2. Calibration standards were prepared in the same acid matrix as the digests. Cu, Fe, Zn, and Se concentrations were expressed as mg/kg sample, while Na content was converted to NaCl percentage using a conversion factor of 2.5 (Regulation EU 1169, 2011).

2.3. Fatty acids profile by GC-FID

Fatty acid methyl esters (FAME) were prepared from approximately 0.2 g of minced fresh or dry-cured Pancetta Piacentina PDO following the direct method of O'Fallon et al. (2007). FAME were analyzed using a Shimadzu GC-FID 2025 system equipped with an AOC-20s autosampler and flame ionization detector (Shimadzu Corporation, Kyoto, Japan), using a CP-Select CB FAME capillary column (100 m × 0.25 mm i.d.; 0.25 μm film thickness; Chrompack, Varian Inc., Palo Alto, CA, USA) and hydrogen as carrier gas at 1.5 mL/min. Injection conditions, injector and detector temperatures, and oven temperature program were as previously reported by Rocchetti et al. (2023). Data were acquired and processed using LabSolutions Lite v5.82 (Shimadzu Srl, Milan, Italy). FAME were identified by comparison with external standards (Supelco 37-component FAME mix, PUFA-3 menhaden oil, and conjugated octadecadienoic acid; Sigma Chemical Co., St. Louis, MO, USA). Results were expressed as percentages of total fatty acids, with peak areas corrected according to AOAC 963.22 (AOAC, 2000).

2.4. Analysis of total peroxides, TBARS, and GSH:GSSG

Peroxide value was determined after cold lipid extraction according to a modified Folch procedure (Christie, 1989), following AOAC Official Method 965.33 (AOAC, 1990). Peroxide values were expressed as milliequivalents of peroxide oxygen per kg of fat (mEq O_2/kg fat). Secondary lipid oxidation was assessed by measuring malondialdehyde (MDA) using the thiobarbituric acid reactive substances (TBARS) assay according to Castro-Cegrí et al. (2023), with slight modifications. Briefly, 0.5 g of sample was homogenized with 7.5 mL of 20% (*w/v*) trichloroacetic acid (TCA) and centrifuged twice at 10,000 ×*g* for 10 min

at 4 °C. An aliquot of the supernatant (0.25 mL) was mixed with 0.75 mL of 0.5% (*w/v*) thiobarbituric acid (TBA), incubated at 94 °C for 30 min, and cooled on ice for 10 min. Absorbance was measured at 532 and 600 nm, and MDA concentrations were expressed as mg MDA equivalents/kg dry weight (DW). Reduced (GSH) and oxidized glutathione (GSSG) were semi-quantified by UHPLC-HRMS using an Orbitrap Exploris 120 mass spectrometer (Thermo Fisher Scientific, Waltham, MA, USA) coupled to a Vanquish UHPLC system, following the untargeted metabolomics workflow described in Section 2.5.1. GSH and GSSG were estimated using calibration curves generated from authentic standards (Sigma-Aldrich) prepared in 80% methanol containing 0.1% formic acid and analyzed under identical instrumental conditions. Calibration curves were constructed over the concentration range of 10–1000 μg/L and showed good linearity ($R^2 = 0.998$ for GSH and $R^2 = 0.9964$ for GSSG). Results were expressed as mg equivalents/kg DW.

2.5. Extraction and UHPLC-HRMS analysis of Pancetta Piacentina PDO samples

2.5.1. Untargeted metabolomics

Metabolites were extracted following Rocchetti et al. (2023). Briefly, 1 g of each Pancetta Piacentina PDO sample was extracted with 10 mL of acidified 80% methanol (*v*/v, containing 0.1% formic acid) using a Polytron™ PT1200E homogenizer (Kinematica, Malters, Switzerland) at 25,000 rpm for 3 min, while maintaining the extraction vessel in an ice bath. Samples were centrifuged at 4227 ×*g* for 15 min at 4 °C, and supernatants were filtered through 0.2 μm cellulose syringe filters into amber vials before UHPLC-HRMS analysis. Samples were extracted on a fresh-weight basis and subsequently normalized to dry matter (DM) during data processing using the corresponding moisture values.

Untargeted metabolomics was performed using an Orbitrap Exploris 120 mass spectrometer (Thermo Fisher Scientific, Waltham, MA, USA) coupled to a Vanquish UHPLC system and equipped with a HESI-II source. Chromatographic separation was achieved using a BEH C18 column (2.1 × 100 mm, 1.7 μm; Waters) with water and acetonitrile (LC-MS grade; Sigma-Aldrich, Milan, Italy), both containing 0.1% formic acid. The gradient increased from 6% to 94% acetonitrile over 35 min at 200 μL/min. Full-scan acquisition was performed in positive ionization mode at a resolving power of 60,000, over *m/z* 75–1125, with a 3 μL injection volume. The AGC target and maximum injection time (IT) were 1×10^6 and 100 ms, respectively. For analytical quality control, a pooled QC sample was prepared by pooling aliquots of all biological sample extracts. Three pooled QC injections, corresponding to 10% of the 30 biological sample injections, were included in the analytical sequence at predefined positions, considering one pooled QC after every 10 samples (González-Domínguez et al., 2024). Sample injection order was randomized to minimize potential analytical bias. Extraction solvent blanks were included in the analytical workflow to remove background-related signals. Pooled QC samples were analyzed using data-dependent acquisition (DDA; Top $N = 4$). MS/MS spectra were acquired at a resolving power of 15,000, with an AGC target of 1×10^5, maximum IT of 100 ms, and 2.0 *m/z* isolation window. Precursors were fragmented using a higher-energy collisional dissociation (HCD) of 23.3%. HESI parameters were: sheath gas, 40 arbitrary units; auxiliary gas, 20 arbitrary units; spray voltage, 3.5 kV; and capillary temperature, 320 °C.

2.5.2. Untargeted lipidomics

Lipid extraction was performed following Rocchetti et al. (2025). Briefly, 0.5 g of each Pancetta Piacentina PDO sample was extracted with 10 mL of tert-butyl methyl ether (MTBE) by ultrasonication for 10 min at 40 kHz and maximum power (Ultrasonic Cleaner Baths, ARGO LAB, Italy), followed by extraction for 10 min at 700 rpm and 4 °C. A hydroalcoholic solution (5 mL; methanol:water, 3:1, *v*/v) was then added, and samples were centrifuged at 5500 rpm for 15 min at 4 °C. One mL of the resulting supernatant was transferred to Eppendorf tubes and evaporated overnight under a fume hood. Dried extracts were reconstituted in 1 mL of 2-propanol:methanol (65:30:5, *v*/v/v). Samples were extracted on a fresh-weight basis and normalized to dry matter (DM) during data processing using the corresponding moisture values.

Untargeted lipidomics was performed using an Orbitrap Exploris 120 mass spectrometer (Thermo Fisher Scientific, Waltham, MA, USA) coupled to a Vanquish UHPLC system and HESI-II source. Chromatographic separation was achieved on a BEH C18 column (2.1 × 100 mm, 1.7 μm; Waters) maintained at 40 °C. The mobile phases consisted of (A) 5 mM ammonium formate and 0.1% formic acid in water/methanol (95/5, *v*/v), and (B) 5 mM ammonium formate and 0.1% formic acid in 2-propanol/methanol/water (65/30/5, *v*/v/v). The elution gradient and chromatographic conditions followed Rocchetti et al. (2025), at a constant flow rate of 200 μL/min. Full-scan acquisition was performed in positive electrospray ionization mode at a resolving power of 60,000, over *m/z* 100–1500, with an AGC target of 1×10^6 and maximum IT of 100 ms. For analytical quality control, a pooled QC sample was prepared and injected as previously described for metabolomic workflow. Sample injection order was randomized to minimize potential analytical bias. Reconstitution solvent blanks were included in the analytical workflow to remove background-related signals. Pooled QC samples were analyzed by data-dependent MS/MS acquisition (Top $N = 4$). MS/MS spectra were acquired at 15,000 resolution, with an AGC target of 1×10^5, maximum IT of 100 ms, and 2.0 *m/z* isolation window. Precursors were fragmented using a higher-energy collisional dissociation (HCD) of 30%. The injection volume was 3 μL. HESI parameters were: sheath gas, 40 arbitrary units; auxiliary gas, 20 arbitrary units; spray voltage, 3.5 kV; and capillary temperature, 320 °C.

2.5.3. Annotation strategies and quality control

Raw metabolomics and lipidomics datasets were processed using MS-DIAL version 4.90 (Tsugawa et al., 2015), including peak detection, gap filling, LOWESS-based signal normalization, and spectral matching. Gap filling was carried out using the Peak Finder algorithm to recover missing peaks, with a tolerance of 5 ppm for *m/z* values. Metabolomics features were annotated against the ESI positive-mode FooDB database and in-house ESI positive-mode spectral libraries, whereas lipidomics features were annotated using the in-house database integrated in LIPIDBLAST. Peak detection was performed over *m/z* 75–1125 and 150–1500 for metabolomics and lipidomics, respectively, with a minimum peak intensity of 10,000 counts per second (cps). Annotation considered accurate mass tolerance (5 ppm), isotopic pattern, MS/MS spectral matching, and an annotation score ≥ 60%. Compound annotation followed the Metabolomics Standards Initiative (MSI) recommendations (Salek et al., 2013). Features supported by accurate mass, isotopic pattern, and MS/MS matching against the corresponding spectral libraries were classified as putatively annotated compounds (MSI Level 2), whereas features assigned only to a chemical class were classified as putatively characterized compound classes (MSI Level 3). To ensure consistency with MSI confidence levels, compound nomenclature was conservatively reported according to the structural information directly supported by the analytical workflow. Thus, positional isomerism, fatty acyl regiochemistry, double-bond location or geometry, hydroxylation sites, and other structural descriptors were not specified when they could not be unequivocally established. Analytical reproducibility was assessed using the relative standard deviation (RSD%) of annotated features across the three pooled QC injections. Features with RSD ≥ 30% were excluded from downstream analyses, following Ghosh et al. (2021). Median QC RSD values were 5.7% and 10.1% for metabolomics and lipidomics, respectively, indicating good analytical repeatability.

2.6. SPME bidimensional (GC × GC)-MS volatile analysis

Two grams of minced sample were transferred into 20-mL headspace vials and analyzed by GC × GC–MS (Shimadzu GCMS-TQ8040 NX,

Kyoto, Japan) equipped with a flow modulator (4 s modulation time), following Leni et al. (2024). Volatiles were extracted by SPME using a DVB/Carbon-WR/PDMS fibre (Restek Srl, Milan, Italy) after equilibration at 40 °C for 20 min under agitation, followed by headspace extraction at 40 °C for 20 min and desorption at 260 °C for 5 min. Separation was performed using a 1D SLB-5 ms column (20 m × 0.18 mm × 0.18 μm; Supelco) coupled to a 2D SupelcoWAX column (5 m × 0.32 mm × 0.25 μm; Supelco). The oven was held at 40 °C for 2 min and then increased to 220 °C at 6 °C/min; mass spectra were acquired over *m/z* 50–650. Data were processed using LabSolutions Post Run (Shimadzu), retaining peaks with S/N > 100 detected in all biological replicates of at least one experimental group. Volatile compounds were putatively identified based on NIST20 mass spectral matching (similarity ≥80%) and comparison of linear retention indices (LRI) calculated using C7–C20 alkanes with values reported in the NIST Chemistry WebBook (Leni et al., 2024). An LRI tolerance of ±2% was applied for compound identification. Volatile compounds were semi-quantified as the $\log_{10}$ of the total integrated chromatographic area divided by the fresh weight of the sample, and the resulting values are reported in Supplementary Table 5 (sheet l). For class-level visualization, the $\log_{10}$-transformed abundance values of individual volatile compounds were summed within each chemical class at each ripening stage, generating a cumulative $\log_{10}$ abundance index. This index was used as a composite measure to compare the relative distribution of volatile classes within each ripening stage and does not represent the total concentration or absolute abundance of a volatile class.

2.7. Sensory analysis of Pancetta Piacentina PDO samples

Sensory profiling was performed by quantitative descriptive analysis (QDA) using a trained panel according to ISO 13299, in an ISO 8589:2007-compliant sensory laboratory at Università Cattolica del Sacro Cuore (Piacenza, Italy). The panel comprised 12 assessors qualified according to the internal validation protocol of Centro Studi Assaggiatori. Panel performance was assessed for repeatability, discrimination, agreement, and overall effectiveness, and only assessors meeting the predefined performance criteria were included in the sensory evaluation. Sensory evaluation was performed on the biological samples collected at T60, T120, T180, and T240, whereas T0 was excluded because the fresh, untreated pork belly was not suitable for direct consumption. Samples were presented to assessors in a randomized and balanced order using blind three-digit codes. A blind replicate of the T240 sample was included to assess panel repeatability. Approximately 1-mm-thick slices were served at 10 °C in individual sensory booths under white lighting. Water and unsalted breadsticks were provided for palate cleansing. Sensory attributes were evaluated using a structured ballot covering visual, olfactory, gustatory, tactile, retronasal aroma, and overall hedonic descriptors, using a 9-point scale. Data were collected using Big Sensory Soft 2.0. Differences among ripening stages were evaluated using Friedman ANOVA followed by non-parametric LSD multiple comparisons, with significance set at $p < 0.05$.

2.8. Statistical analysis and data integration

Statistical analyses of proximate composition, redox parameters, fatty acid profiles, and volatile profiles were performed using R (version 4.4.1). Differences among ripening stages were assessed by one-way ANOVA followed by Duncan's post hoc test ($p < 0.05$). For volatile profiles, Duncan's post hoc comparisons were additionally used to compare chemical classes within each ripening stage, whereas temporal variation within each volatile class was assessed separately by one-way ANOVA. Metabolomics and lipidomics data were normalized to dry matter (DM) based on sample moisture. Multivariate analyses were performed using MetaboAnalyst 6.0 (Pang et al., 2024) after $\log_{10}$ transformation, median-centering, and Pareto scaling, including HCA, PCA, sPLS-DA, and OPLS-DA. sPLS-DA models were assessed by 5-fold cross-validation. OPLS-DA models compared T0 (fresh, untreated pork belly) with each ripening stage and were evaluated using R^2X, R^2Y, Q^2, and 100-permutation tests. Given the limited number of biological replicates relative to dataset dimensionality, OPLS-DA models were considered exploratory and not predictive of independent samples. Discriminant features were selected using VIP >1, while differential features were identified by Volcano analysis (FC >1.2, ANOVA $p < 0.05$, FDR correction). Individual-feature ROC/AUC analysis was performed using the Classical univariate ROC workflow in MetaboAnalyst 6.0 and was considered exploratory given the limited sample size. Formal integration of metabolomics and lipidomics was performed using supervised DIABLO in mixOmics R (version 6.26). Data were mean-centered and unit variance-scaled, and a three-component `block.splsda` model (`ncomp = 3`) was fitted with ripening stage as the response. Variable selection was optimized by repeated M-fold cross-validation, resulting in `keepX = 10` variables per block. Model performance was evaluated by repeated 3-fold cross-validation (50 repeats) using Mahalanobis distance. Score and correlation plots were used to visualize stage discrimination and associations between selected variables. Given the supervised nature of DIABLO, these associations were interpreted as model-derived relationships contributing to stage discrimination rather than independent evidence of biological coordination. Volatile and sensory data were not formally integrated and were considered complementary analytical layers.

3. Results and discussion

3.1. Proximate and mineral composition of Pancetta Piacentina PDO samples

The evolution of proximate composition during Pancetta Piacentina PDO ripening is reported in Supplementary Table 3. As expected for dry-cured meat products, moisture content progressively decreased from 40.2 g/100 g at T0 to 30.5 g/100 g at T240, reflecting the water loss occurring during curing and drying, a key process for product stabilization and shelf-life (Mediani et al., 2022). Accordingly, protein content increased during ripening, reaching 18.4 g/100 g at T180, mainly as a consequence of dehydration and concentration of nitrogenous compounds (Vasconcelos et al., 2025), although a slight decrease was observed at T240. In contrast, total lipid content remained relatively stable (approximately 45–50 g/100 g), despite the extensive qualitative changes in lipid composition documented by fatty acid profiling, oxidative markers, and lipidomics. Ash content increased markedly from 0.6 g/100 g at T0 to >4 g/100 g at advanced ripening stages, consistently with salt penetration and diffusion into the meat matrix (Ferreira et al., 2013). NaCl content increased from 0.09 g/100 g in fresh meat to approximately 2–3 g/100 g in ripened samples, with the highest value at T180. Salt diffusion contributes to microbial stability, protein solubilization, and flavor development (Jia et al., 2024), while also promoting dehydration, modifying water-holding capacity, and contributing to the characteristic firmness and texture of dry-cured meats (Domínguez, Pateiro, et al., 2019). Moreover, NaCl can modulate the perception and release of aroma compounds generated during proteolysis and lipolysis, thereby contributing to the sensory characteristics of the final product (Liang et al., 2025). Mineral composition is reported in Supplementary Table 4. Cu, Fe, and Se did not vary significantly throughout ripening ($p > 0.05$), whereas Zn increased progressively up to T180 before decreasing at T240. This pattern may reflect both concentration effects associated with moisture loss and the release of mineral elements from muscle proteins during proteolysis (Adamsen et al., 2006). Taken together, the compositional changes observed during ripening reflect the combined effects of dehydration, salt diffusion, and progressive biochemical transformations characteristic of dry-cured meat products.

3.2. Modification of fatty acid profile during ripening time

The fatty acid composition of Pancetta Piacentina PDO during ripening is reported in Table 1. The lipid fraction was dominated by MUFA, followed by SFA and PUFA, consistent with the typical composition of pork adipose tissue (Domaradzki et al., 2022). Oleic acid (C18:1n9c) was the most abundant fatty acid throughout ripening (~44%) and did not vary significantly, while palmitic (C16:0) and stearic (C18:0) acids were the predominant SFA. Palmitic acid showed a slight but significant relative increase, reaching its highest values at T120 and T180. Given that data are expressed as percentages of total fatty acids, this relative increase may partly reflect changes in the proportion of other fatty acid groups rather than absolute accumulation (Zhang et al., 2026). PUFA showed the most pronounced change, decreasing significantly from 12.30% at T0 to values between 8.86 and 10.18% in the ripened samples (T60–T240), with no significant differences among ripening stages. Linoleic acid (C18:2n6c), together with several long-chain PUFA (C20:2, C20:3n6, C20:3n3, C22:5n3, and C22:6n3), also showed lower relative proportions during ripening, although the magnitude and statistical significance of these changes varied among individual fatty acids. The relative SFA proportion increased significantly from T0 to T120–T180, whereas MUFA remained comparatively stable throughout ripening. Similar changes have been reported in traditional dry-cured beef products (Sha et al., 2016), supporting the occurrence of lipid remodeling during maturation, although the specific contribution of oxidative and enzymatic processes was not directly assessed in the present study (Domínguez, Pateiro, et al., 2019; Seong et al., 2015; Zhang et al., 2026). The reduction in the relative proportion of PUFA may be associated with the formation of secondary lipid oxidation products, including aldehydes, alcohols, and ketones, which have been reported to contribute to the characteristic aroma and flavor of dry-cured meats (Yu & Gu, 2025). However, the present study did not directly establish precursor–product relationships between individual fatty acids and volatile compounds. Overall, the fatty acid profile provides evidence of changes in lipid composition during Pancetta Piacentina PDO ripening and complements the oxidative and volatile transformations described below.

3.3. Evolution of redox markers (TBARS, peroxides, GSH:GSSG ratio)

The evolution of oxidative markers during Pancetta Piacentina PDO ripening is reported in Table 2. Overall, ripening was associated with marked changes in lipid oxidation markers and in the glutathione system, although the temporal patterns differed among the individual parameters. Peroxide values increased significantly from 1.7 mEq O_2/kg fat at T0 to 11.8 at T60, reaching the highest value at T120 (20.9 mEq O_2/kg fat), and subsequently decreased at T180 and T240. T60 and T180 did not differ significantly, whereas T120 showed the highest peroxide value. This pattern is consistent with the formation of primary lipid oxidation products during ripening, followed by their subsequent decomposition or conversion into secondary oxidation products. Oxygen exposure, endogenous pro-oxidant catalysts such as heme iron, and the presence of unsaturated fatty acids may contribute to hydroperoxide formation during dry-curing (Tatiyaborworntham et al., 2022). However, these mechanisms were not directly investigated in the present study. TBARS showed a related but not identical temporal pattern. Values increased significantly from 0.6 mg MDA/kg DM at T0 to 1.4 and 1.3 mg MDA/kg DM at T60 and T120, respectively, whereas the value at T240 (0.8 mg MDA/kg DM) was not significantly different from T0. T60 and T120 showed comparable TBARS concentrations despite the continued increase in peroxide values, indicating that the accumulation of primary and secondary oxidation products did not occur in parallel.

Table 1
Fatty acid composition of Pancetta Piacentina PDO samples during ripening, expressed as percentage of total fatty acid methyl esters (FAME). Results represent the mean of six independent replicates ($n = 6$). Different superscript letters within the same row indicate significant differences among ripening times according to one-way ANOVA followed by Duncan's multiple range test ($p < 0.05$).

Fatty acids	T0	T60	T120	T180	T240
C 8:0	0.009 ± 0.000^{a}	0.007 ± 0.001^{b}	0.006 ± 0.001^{c}	0.008 ± 0.001^{ab}	0.008 ± 0.001^{ab}
C 10:0	0.072 ± 0.003^{a}	0.066 ± 0.004^{b}	0.063 ± 0.006^{b}	0.075 ± 0.003^{a}	0.066 ± 0.005^{b}
C 12:0	0.07 ± 0.01	0.07 ± 0.00	0.07 ± 0.01	0.07 ± 0.00	0.06 ± 0.01
C 14:0	1.14 ± 0.10^{c}	1.30 ± 0.08^{ab}	1.42 ± 0.14^{a}	1.41 ± 0.06^{a}	1.25 ± 0.11^{bc}
C 14:1	0.010 ± 0.001^{b}	0.014 ± 0.003^{a}	0.016 ± 0.003^{a}	0.017 ± 0.002^{a}	0.014 ± 0.003^{a}
C 15:0	0.04 ± 0.00	0.03 ± 0.01	0.03 ± 0.01	0.03 ± 0.00	0.04 ± 0.01
C 16:0	24.15 ± 0.94^{b}	25.15 ± 0.94^{ab}	25.86 ± 0.99^{a}	26.17 ± 0.48^{a}	25.48 ± 1.14^{a}
C 16:1	1.93 ± 0.15	2.39 ± 0.46	2.34 ± 0.25	2.50 ± 0.30	1.90 ± 0.85
C 17:0	0.24 ± 0.03	0.21 ± 0.07	0.19 ± 0.03	0.20 ± 0.02	0.23 ± 0.07
C 18:0	12.17 ± 0.40	11.82 ± 1.02	12.58 ± 0.82	12.53 ± 0.52	12.33 ± 0.92
C 18:1n9c	44.12 ± 1.05	44.44 ± 0.92	43.67 ± 1.51	43.83 ± 0.39	44.49 ± 1.40
C 18:1cis11	2.75 ± 0.09^{b}	3.22 ± 0.36^{a}	3.17 ± 0.18^{a}	3.26 ± 0.21^{a}	3.12 ± 0.28^{a}
C 18:2n6c	10.71 ± 1.48^{a}	8.85 ± 0.89^{b}	8.29 ± 0.72^{b}	7.72 ± 0.78^{b}	8.66 ± 0.82^{b}
C 18:3n6	0.06 ± 0.01^{a}	0.02 ± 0.00^{b}	0.02 ± 0.00^{b}	0.02 ± 0.00^{b}	0.05 ± 0.03^{a}
C 18:3n3	0.40 ± 0.05^{a}	0.34 ± 0.04^{b}	0.33 ± 0.04^{b}	0.31 ± 0.03^{b}	0.33 ± 0.04^{b}
C 20:0	0.15 ± 0.01^{b}	0.18 ± 0.03^{ab}	0.19 ± 0.02^{a}	0.17 ± 0.01^{ab}	0.16 ± 0.02^{b}
CLA tot.	0.07 ± 0.01	0.09 ± 0.03	0.06 ± 0.01	0.06 ± 0.01	0.09 ± 0.05
C 20:1	0.83 ± 0.08	0.89 ± 0.10	0.88 ± 0.07	0.81 ± 0.07	0.83 ± 0.15
C 20:2	0.51 ± 0.04^{a}	0.45 ± 0.07^{b}	0.40 ± 0.05^{bc}	0.36 ± 0.04^{c}	0.40 ± 0.04^{bc}
C 20:3n6	0.08 ± 0.01^{a}	0.07 ± 0.01^{b}	0.06 ± 0.01^{bc}	0.06 ± 0.01^{c}	0.07 ± 0.01^{b}
C 20:3n3	0.08 ± 0.01^{a}	0.08 ± 0.01^{ab}	0.07 ± 0.01^{bc}	0.06 ± 0.01^{c}	0.07 ± 0.01^{bc}
C 20:4n6	0.29 ± 0.02^{a}	0.22 ± 0.03^{bc}	0.20 ± 0.01^{c}	0.22 ± 0.02^{c}	0.25 ± 0.05^{ab}
C 22:0	0.01 ± 0.00^{b}	0.01 ± 0.00^{b}	0.01 ± 0.00^{b}	0.04 ± 0.00^{a}	0.01 ± 0.00^{b}
C 22:1n9	0.01 ± 0.00	0.01 ± 0.00	0.01 ± 0.00	0.01 ± 0.00	0.01 ± 0.00
C 20:5n3	0.01 ± 0.00	0.01 ± 0.00	0.01 ± 0.00	0.01 ± 0.00	0.01 ± 0.00
C 22:5n3	0.06 ± 0.00^{a}	0.05 ± 0.01^{b}	0.05 ± 0.00^{bc}	0.04 ± 0.00^{c}	0.05 ± 0.01^{bc}
C 22:6n3	0.019 ± 0.002^{a}	0.008 ± 0.003^{c}	0.007 ± 0.001^{c}	0.009 ± 0.001^{bc}	0.011 ± 0.004^{b}
SFA	38.04 ± 1.46^{c}	38.85 ± 1.56^{bc}	40.42 ± 1.59^{ab}	40.71 ± 0.64^{a}	39.64 ± 1.65^{abc}
MUFA	49.66 ± 1.09	50.97 ± 1.21	50.09 ± 1.34	50.43 ± 0.60	50.37 ± 1.88
PUFA	12.30 ± 1.57^{a}	10.18 ± 1.02^{b}	9.49 ± 0.80^{b}	8.86 ± 0.88^{b}	9.99 ± 0.90^{b}
UFA	61.96 ± 1.46^{a}	61.15 ± 1.56^{ab}	59.58 ± 1.59^{bc}	59.29 ± 0.64^{c}	60.36 ± 1.65^{abc}

Abbreviations: SFA, saturated fatty acids; MUFA, monounsaturated fatty acids; PUFA, polyunsaturated fatty acids; UFA, unsaturated fatty acids; T0 (fresh, untreated pork belly); T60 (60-days ripening); T120 (120-days ripening); T180 (180-days ripening); T240 (240-days ripening).

Table 2
Effect of ripening time on peroxide value, TBARS, GSH, GSSG, and GSH:GSSG ratio of Pancetta Piacentina PDO. Results are expressed as mean ± standard deviation, considering six independent biological replicates ($n = 6$). Different superscript letters within each column indicate significant differences among ripening times according to one-way ANOVA followed by Duncan's multiple range test ($p < 0.05$).

Sample	Peroxide value (m.eq. O_2/kg fat)	TBARS (mg MDA/kg DM)	GSH (mg/kg DM)	GSSG (mg/kg DM)	GSH:GSSG
T0	1.7 ± 1.0^{d}	0.6 ± 0.3^{c}	225.6 ± 67.2^{a}	1.6 ± 0.4^{bc}	152.8 ± 69.8^{a}
T60	11.8 ± 1.8^{c}	1.4 ± 0.6^{a}	34.1 ± 16.2^{b}	7.7 ± 5.5^{a}	5.0 ± 1.6^{b}
T120	20.9 ± 4.4^{a}	1.3 ± 0.6^{a}	28.2 ± 6.3^{b}	3.9 ± 0.3^{b}	7.3 ± 2.0^{b}
T180	13.4 ± 2.1^{c}	1.2 ± 0.5^{ab}	20.0 ± 7.0^{b}	1.7 ± 1.3^{bc}	19.4 ± 12.2^{b}
T240	16.2 ± 1.9^{b}	0.8 ± 0.2^{bc}	10.9 ± 3.6^{b}	0.6 ± 0.1^{c}	19.5 ± 6.2^{b}
Sig.	***	**	***	***	***

Abbreviations: TBARS: Thiobarbituric Acid Reactive Substances; GSH: Glutathione; GSSG: Glutathione Disulfide. Sig.: significance; *** = $p < 0.001$; ** = $p < 0.01$; T0 (fresh, untreated pork belly); T60 (60-days ripening); T120 (120-days ripening); T180 (180-days ripening); T240 (240-days ripening).

This may reflect the subsequent conversion, degradation, or interactions of secondary oxidation products with proteins, peptides, and amino acids (Zhu et al., 2022). Since TBARS measures only a subset of secondary lipid oxidation products, its evolution does not necessarily parallel peroxide formation (Reitznerová et al., 2017). Similar temporal differences between primary and secondary oxidation markers have been reported in other ripened PDO meat products (Rocchetti et al., 2025). Overall, the decrease in peroxide and TBARS values observed during advanced ripening may be consistent with the instability and further transformation of lipid oxidation products, although the specific reaction pathways were not directly assessed. The glutathione system also showed substantial changes during ripening. GSH, an important endogenous antioxidant in muscle tissue (Baldelli et al., 2019), decreased markedly from 225.6 mg equivalents/kg DM at T0 to 34.1 at T60 and 10.9 at T240. However, all ripened stages (T60–T240) belonged to the same statistical group, indicating that the significant difference was primarily between the fresh baseline and the ripened samples rather than among the individual ripening stages. The observed reduction is consistent with consumption or transformation of GSH during oxidative processes, including reactions involving reactive oxygen species and lipid-derived oxidants (Dragoev, 2024). Other processes, such as γ-glutamyltransferase-mediated degradation or microbial metabolism, may also contribute to changes in glutathione levels, but their relative contribution was not directly investigated. GSSG increased from 1.6 mg equivalents/kg DM at T0 to 7.7 at T60, followed by a progressive numerical decrease to 3.9, 1.7, and 0.6 mg equivalents/kg DM at T120, T180, and T240, respectively. The highest GSSG concentration was observed at T60, whereas T240 showed the lowest value. The early increase in GSSG is compatible with oxidation of GSH to its disulfide form (Aquilano et al., 2014), while the subsequent decrease may reflect further transformation or turnover of glutathione-derived compounds. These mechanisms remain hypothetical because glutathione turnover pathways were not directly measured. Accordingly, the semi-quantitative GSH:GSSG ratio decreased sharply from 152.8 at T0 to 5.0 at T60. Although the ratio subsequently increased numerically to approximately 19.5 at T180–T240, all ripened stages remained significantly lower than T0 and did not differ significantly from one another. The later increase in the ratio should therefore not be interpreted as a restoration of antioxidant capacity, but rather as the result of the proportionally greater decline in GSSG relative to GSH. A different pattern was reported by Marušić et al. (2013), who observed a progressive decline in both GSH and GSSG during six months of ham dry-curing. Because GSH and GSSG were semi-quantified within the untargeted metabolomics workflow, these results should be considered indicative of changes in glutathione-associated metabolism rather than fully validated quantitative measurements of absolute redox status. The redox data indicate a pronounced difference between fresh untreated pork belly and the ripened product, characterized by increased peroxide and TBARS values during the early stages and substantial alteration of the glutathione system. The subsequent decline in peroxide and TBARS values during advanced ripening suggests further transformation of oxidation products, while the persistently low GSH:GSSG ratio indicates that the glutathione system remained markedly altered relative to T0. These observations provide complementary evidence for redox-related transformations during Pancetta Piacentina PDO ripening, without establishing specific biochemical mechanisms or direct precursor–product relationships with individual volatile compounds.

3.4. Integration of metabolomics and lipidomics to evaluate biochemical modifications

3.4.1. Untargeted metabolomics

The untargeted UHPLC-HRMS workflow allowed the putative annotation of 2316 mass features after quality filtering (RSD <30%, signal-to-noise ratio > 10, and annotation score; Supplementary Table 5, sheet a). Among these, 83 metabolites were putatively annotated at MSI Level 2 through MS/MS spectral matching against FooDB, whereas the remaining features were assigned to putatively characterized compound classes (MSI Level 3). Amino acids, peptides and analogues represented the largest chemical class (255 features), followed by carbohydrate conjugates (100), triterpenoids (61), carbonyl compounds (40), and several fatty acid derivatives. Given the predominance of MSI Level 3 annotations, these results provide an overview of the major putatively assigned chemical classes rather than definitive structural identification. Accordingly, the biochemical interpretations below should be considered at the level of molecular trends rather than definitive mechanistic evidence for individual compounds (Supplementary Table 5, sheet a). HCA and PCA clearly discriminated samples according to ripening stage (Supplementary Table 5, sheet c). HCA separated fresh samples (T0) from ripened samples (T60–T240), with T180 and T240 showing further differentiation. PCA confirmed this progressive biochemical evolution, with PC1 and PC2 explaining 77.7% of the total variance. sPLS-DA further showed three major metabolic clusters corresponding to T0, T60, and T120–T240, highlighting T60 as a key metabolic transition between the fresh and ripened product.

OPLS-DA models were subsequently generated independently for each ripening stage versus T0. Discriminant metabolites were selected by integrating VIP values, Volcano plot analysis, and univariate ROC analysis (Supplementary Table 5, sheet d). The T60 vs T0 comparison yielded 458 discriminant metabolites based on the predefined selection criteria. Among the most discriminant features (VIP >2; all adjusted $p <$ 0.01), thesinine (MSI Level 3; $\log_2FC = 13.08$), pheophorbide a (MSI Level 3; $\log_2FC = 12.86$), isopiperine (MSI Level 2; $\log_2FC = 12.92$), gartanin (MSI Level 3; $\log_2FC = 11.34$), glutaminyltyrosine (MSI Level 3; $\log_2FC = 10.88$), and hydroxy-octadecenoylcarnitine (MSI Level 3; $\log_2FC = -11.61$) showed the strongest discrimination. Several of these features were putatively annotated as plant-derived secondary metabolites, potentially reflecting contributions from spices used during PDO processing, which permits black and/or white pepper and cloves (Commission Regulation EC No. 1263/96). Because the exact spice formulation used for the investigated batch was unavailable, this interpretation remains hypothetical. Importantly, 23 of the discriminant features in the T60 vs T0 comparison were supported by MS/MS spectral matching (MSI Level 2; Supplementary Table 5, sheet d). Several of these metabolites were dipeptides, including L-prolyl-*L*-phenylalanine, glycyl-glutamine, aspartyl-isoleucine, alanyltryptophan, and phenylalanyl-glycine, all of which increased significantly at T60. Their

accumulation is consistent with the progressive proteolytic activity occurring during dry-cured meat maturation (Mora et al., 2015), potentially reflecting the sequential hydrolysis of muscle proteins and larger peptide intermediates and contributing to the pool of low-molecular-weight nitrogenous compounds that can subsequently undergo further transformation. These MS/MS-supported changes therefore provide additional evidence of proteolytic remodeling during the early stages of Pancetta Piacentina PDO ripening.

The T120 vs T0, T180 vs T0, and T240 vs T0 comparisons yielded 513, 539, and 582 discriminant metabolites, respectively. The features putatively annotated as quercetin-acetylglucoside (MSI Level 3; RSD = 1.4%) and hydroxy-octadecenoylcarnitine were consistently among the most discriminant features (VIP >2) and showed progressive reduction during ripening. The decrease in quercetin-acetylglucoside, a flavonoid glycoside, may be associated with transformations occurring during ripening, whereas the reduction of hydroxy-octadecenoylcarnitine may reflect lipid remodeling, consistent with the fatty acid and lipidomics results. Given their annotation confidence, however, these interpretations remain putative. MS/MS-supported annotations provided additional evidence for specific metabolic changes at the different ripening stages. At T120, 17 discriminant features were assigned to MSI Level 2 (Supplementary Table 5, sheet d). Several were related to amino acid and peptide metabolism, including alanylasparagine, histidinyl-alanine, L-histidine, alanyltryptophan, and L-prolyl-*L*-phenylalanine. Their marked changes, together with the peptide accumulation observed at T60, are consistent with continued remodeling of the low-molecular-weight nitrogen fraction during ripening. Other Level 2 metabolites, including 12-oxo-PDA and monoacylglycerol MG(0:0/18:1(11Z)/0:0), increased at T120, providing additional evidence of lipid-related changes. Notably, isopiperine showed one of the highest VIP scores among the Level 2 features at this stage (VIP = 1.93; $\log_2$FC = 11.77), together with other putatively identified compounds potentially associated with plant-derived material. At T180, 20 discriminant features were supported by MS/MS spectral matching (MSI Level 2). The pattern observed at T120 was largely maintained, with increases in L-prolyl-*L*-phenylalanine, asparaginyl-γ-glutamate, and alanyltryptophan, whereas alanylasparagine, histidinyl-alanine, and L-histidine decreased. This divergent pattern further supports continued remodeling of the low-molecular-weight nitrogen fraction rather than a generalized accumulation of peptide metabolites. In parallel, MG(0:0/18:1(11Z)/0:0) and α-dimorphecolic acid increased, providing additional MS/MS-supported evidence of lipid remodeling and oxidation-related changes. Isopiperine remained one of the most discriminant Level 2 features at T180 (VIP = 1.97; $\log_2$FC = 12.30), together with (*R*)-3,7-dimethyl-5-indanecarboxylic acid (VIP = 1.94; $\log_2$FC = 12.04). At T240, 20 discriminant features were likewise supported by MS/MS spectral matching (MSI Level 2). Several peptide- and amino acid-related metabolites increased, including alanyltryptophan, asparaginyl-γ-glutamate, and L-prolyl-*L*-phenylalanine, whereas betaine, L-histidine, alanylasparagine, histidinyl-alanine, and β-guanidinopropionic acid decreased. This pattern indicates continued remodeling of the low-molecular-weight nitrogen fraction during prolonged maturation. In parallel, MG(0:0/18:1(11Z)/0:0), (*R*)-2-hydroxysterculic acid, and 12-oxo-PDA increased, further supporting lipid-related changes during advanced ripening. Notably, isopiperine and (*R*)-3,7-dimethyl-5-indanecarboxylic acid remained among the most discriminant Level 2 features at T240 (VIP = 1.86 and 1.83; $\log_2$FC = 11.73 and 11.53, respectively). The persistent accumulation of isopiperine from T120 onward may be consistent with a contribution from plant-derived spices used during processing, although the specific spice formulation of the investigated batch was unavailable and this hypothesis cannot be confirmed from the present data.

The progressive changes in MS/MS-supported metabolites were complemented by several T240-associated Level 3 features. Venn analysis identified 144 putatively annotated metabolites uniquely associated with T60, 119 with T240, 54 with T120, and 46 with T180, whereas approximately 23% of the discriminant metabolites (~213 features) were shared among comparisons (Supplementary Table 5, sheet e). The distinct metabolomic signatures of T60 and T240 further support their role as key transition points in the ripening process. Among the relatively small number of metabolites supported by MS/MS spectral matching, betaine was uniquely discriminant in the T240 vs T0 comparison and showed a marked decrease during ripening ($\log_2$FC = −3.48; adjusted $p = 2.76 \times 10^{-5}$; VIP = 1.01; univariate AUC = 1.00; RSD = 10.9%). Betaine is a naturally occurring zwitterionic compound involved in cellular osmotic regulation and methyl-group metabolism (Liu et al., 2026), and its depletion may reflect biochemical transformations occurring during prolonged ripening. However, the specific processes underlying this decrease cannot be established from the present untargeted data and would require targeted quantitative analyses and complementary investigation of related metabolites. Among the Level 3 features, a feature putatively annotated as homoglutathione ($\log_2$FC = 8.48; RSD = 4.6%; adjusted $p < 0.01$) showed exclusive and marked accumulation at T240. This glutathione analogue is more commonly reported in plants and microorganisms than in animal tissues (Colville et al., 2015). Because its annotation was based on putative characterization rather than definitive structural identification, its potential association with curing-associated microbial or glutathione-related transformations should be considered hypothetical and requires confirmation by targeted analysis. Several other discriminant features were also consistent with potential lipid oxidation and remodeling. Putatively annotated hydroxylated fatty acids, including hydroxy-dodecanedioic acid (MSI Level 3; RSD = 0.6%) and hydroxy-trioxooctadecanoic acid (MSI Level 3; RSD = 8.9%), have been associated with advanced lipid oxidation (Xia & Budge, 2018), while hydroxy-octadecatetraynoic acid (MSI Level 3; RSD = 6.8%) and hydroxylated leukotriene E4 (MSI Level 3; RSD = 2.0%) may represent oxylipin-like features associated with enzymatic or non-enzymatic PUFA oxidation (Dyall et al., 2022). Such changes are consistent with the simultaneous lipolysis and oxidation characteristic of dry-cured meat maturation (Seo et al., 2024). Likewise, putatively annotated lysophospholipid features (MSI Level 3), including LysoPE(0:0/22:0) and LPA(20:1/0:0), were strongly associated with T240 and may reflect phospholipase-mediated membrane lipid hydrolysis and microbial enzymatic activity (Tatiyaborworntham et al., 2022), potentially contributing to free fatty acid release and subsequent oxidation. Putatively annotated sterol-related compounds, including dehydrocholesterol and methylene cholesterol, also increased during prolonged ripening, potentially reflecting oxidative or enzymatic cholesterol transformations (Domínguez, Pateiro, et al., 2019). Finally, putative Level 3 features such as citrulline and the dipeptide asparaginylaspartic acid were exclusively associated with T240 and may reflect progressive proteolysis and subsequent amino acid metabolism (Heres et al., 2023), processes that contribute to flavor development through the generation of free amino acids and peptides. Other discriminant putatively annotated compounds, including methylthioribosyl-zeatin and several terpene- and phenolic-like features, may be associated with microbial metabolism or with transformations involving lipid-, amino acid-, and plant-derived compounds. All OPLS-DA models showed high R^2Y and Q^2 values, while 100-permutation testing yielded empirical $p < 0.01$ for both parameters (Supplementary Table 5, sheet d). These results indicate that the observed class separation was greater than that obtained after random permutation of class labels. However, given the limited number of biological replicates relative to the high dimensionality of the omics datasets, the supervised OPLS-DA models were considered exploratory, and their performance should not be interpreted as evidence of generalizability to independent samples. Similarly, univariate ROC/AUC results were used as an exploratory criterion for individual-feature discrimination and were not considered evidence of predictive biomarker performance. Collectively, the untargeted metabolomics data reveal extensive biochemical remodeling throughout Pancetta Piacentina PDO ripening, encompassing changes in the low-molecular-weight nitrogen fraction, lipid remodeling and oxidation, and putative

contributions from microbial metabolism and plant-derived ingredients. The MS/MS-supported Level 2 features provide additional evidence for these trends, while the broader Level 3 dataset offers complementary information on the chemical classes involved.

3.4.2. Untargeted lipidomics

Untargeted UHPLC-HRMS lipidomics allowed the putative annotation of lipid species after applying the same quality filters used for metabolomics (RSD <30%, signal-to-noise ratio > 10, and annotation score; Supplementary Table 5, sheet f). Among the retained features, 113 lipid species were putatively annotated at MSI Level 2 through MS/MS matching against the LIPIDBLAST library, whereas the remaining features were assigned to putatively characterized lipid classes (MSI Level 3). The main putatively assigned classes were sphingolipids (1026 features), glycerolipids (555), fatty acyls (551), glycerophospholipids (500), sterol lipids (79), and prenol lipids (54). Structural interpretations were restricted to the confidence level supported by the analytical workflow. HCA mainly separated fresh (T0) from ripened samples and further identified distinct lipidomic profiles for T60 and T240 (Supplementary Table 5, sheet h). PCA explained 60.6% of the total variance through PC1 and PC2, while sPLS-DA confirmed the ability of the lipidomic dataset to discriminate ripening stages. To characterize lipid remodeling at the lipid-class level independently of feature selection by supervised analyses, median log_2FC values were calculated across the complete set of quality-filtered lipid features assigned to each lipid category, using the relative peak areas normalized to dry matter (Table 3). Fatty acyls showed positive median log_2FC values across all ripening stages, increasing from 0.21 at T60 to 0.43 at T240. Glycerolipids similarly showed positive median log_2FC values, ranging from 0.31 at T60 to 0.46 at T240. Sphingolipids also remained consistently above T0, with median log_2FC values ranging from 0.20 to 0.32. Prenol lipids showed the largest positive class-level changes, increasing from 0.91 at T60 to 2.02 at T240, whereas sterol lipids showed progressively positive changes from 0.01 at T60 to 0.45 at T240. Glycerophospholipids showed a different temporal pattern, with a median log_2FC of −0.05 at T60, a small positive value at T120 (0.08), and progressively negative values at T180 (−0.07) and T240 (−0.10). Overall, these class-level trends indicate progressive remodeling of lipid composition during ripening, with positive changes in several lipid categories and a relative reduction of glycerophospholipids during advanced maturation. The class-level patterns were complemented by feature-level supervised analyses. OPLS-DA models identified discriminant lipid features for each ripening stage versus T0, with the selected features and their corresponding VIP values, fold changes, statistical significance, and AUC values reported in Supplementary Table 5 (sheet i). Among the most discriminant features at T240, SM 58:7;3O and SM 12:0;2O/16:0 (both annotated as MSI level 3) showed marked increases. These putative sphingomyelin features are consistent with the overall positive trend observed for the sphingolipid class. Sphingomyelins are major membrane constituents and are generally less susceptible to oxidation than glycerophospholipids (Li et al., 2026); therefore, their relative increase may partly reflect the preferential depletion of more oxidation-prone phospholipids. Their involvement in membrane homeostasis and cellular stress responses may also be relevant during prolonged curing (Breslow & Weissman, 2010). However, these mechanistic interpretations remain putative given the untargeted nature of the analysis. The positive class-level trend observed for fatty acyls is consistent with progressive hydrolysis of triglycerides and phospholipids and the release of free fatty acids and related derivatives (Domínguez, Pateiro, et al., 2019). These compounds may provide substrates for subsequent oxidative reactions and contribute to volatile formation during dry-cured meat maturation (Zhang et al., 2026). The increase in glycerolipids may reflect triglyceride remodeling through endogenous lipases, salt-promoted hydrolysis, and microbial enzymatic activity (Zhang et al., 2026; Zhao et al., 2020). Conversely, the negative median log_2FC observed for glycerophospholipids at T180 and T240 is consistent with progressive phospholipid remodeling during maturation. Given the high PUFA content of several glycerophospholipid species, their reduction may also be related to their susceptibility to oxidation (Dragoev, 2024), potentially contributing to the fatty acid-derived oxidation products detected by metabolomics. Prenol and sterol lipids showed positive class-level changes during ripening. Prenol lipids were mainly represented by vitamin A esters (retinyl esters), whereas sterol lipids included mainly sterol esters and acyl steryl glycosides. These changes may reflect remodeling of minor lipid constituents and oxidative modifications of lipid-soluble compounds, although such interpretations remain putative given the untargeted annotation strategy. At the feature level, the highest numbers of stage-specific VIP lipids were observed at T240 (69 lipids) and T60 (59 lipids), while approximately 35% of discriminant lipids (261 compounds) were shared across pairwise comparisons (Supplementary Table 5, sheet j). This pattern indicates that the lipidomic dataset captured both early and late stage-specific molecular changes during ripening. Pancetta Piacentina PDO ripening was then characterized by a progressive remodeling of lipid composition, with positive class-level changes in fatty acyls, glycerolipids, sphingolipids, prenol lipids, and sterol lipids, together with a relative reduction of glycerophospholipids during advanced maturation. These global class-level trends were complemented by specific discriminant lipid features identified by supervised analyses, providing a more detailed view of lipidomic changes throughout ripening.

3.4.3. Metabolomic and lipidomic data fusion

Metabolomics and lipidomics datasets were integrated using the supervised DIABLO framework to investigate relationships between the two molecular layers in relation to Pancetta Piacentina PDO ripening. Classification error decreased across components from 0.0367 to 0.0133 for metabolomics and from 0.154 to 0.097 for lipidomics, indicating low classification error and consistent discriminative performance across the two omics blocks. The first latent components showed a very strong correlation (r = 0.98; Fig. 1A). Because DIABLO is supervised by ripening stage, this correlation represents a model-derived association between the two omics datasets contributing to sample discrimination and should not be interpreted as independent evidence of biological coordination. The top discriminant variables (Fig. 1B) included peptides

Table 3
Median log_2 fold changes (log_2FC) of lipidomic features within each lipid category during Pancetta Piacentina PDO ripening. For each lipid category, median log_2FC values were calculated across the fixed set of quality-filtered lipid features assigned to that category, using relative peak areas normalized to dry matter. The same feature set was considered across ripening-stage comparisons.

Lipid category	n° features	median log_2FC T60 vs T0	median log_2FC T120 vs T0	median log_2FC T180 vs T0	median log_2FC T240 vs T0
Fatty acyls	551	0.21	0.40	0.35	0.43
Glycerolipids	555	0.31	0.53	0.49	0.46
Glycerophospholipids	500	−0.05	0.08	−0.07	−0.10
Prenol lipids	54	0.91	1.61	1.98	2.02
Sphingolipids	1026	0.20	0.32	0.24	0.29
Sterol lipids	79	0.01	0.27	0.42	0.45

Abbreviations: T0 (fresh, untreated pork belly); T60 (60-days ripening); T120 (120-days ripening); T180 (180-days ripening); T240 (240-days ripening).

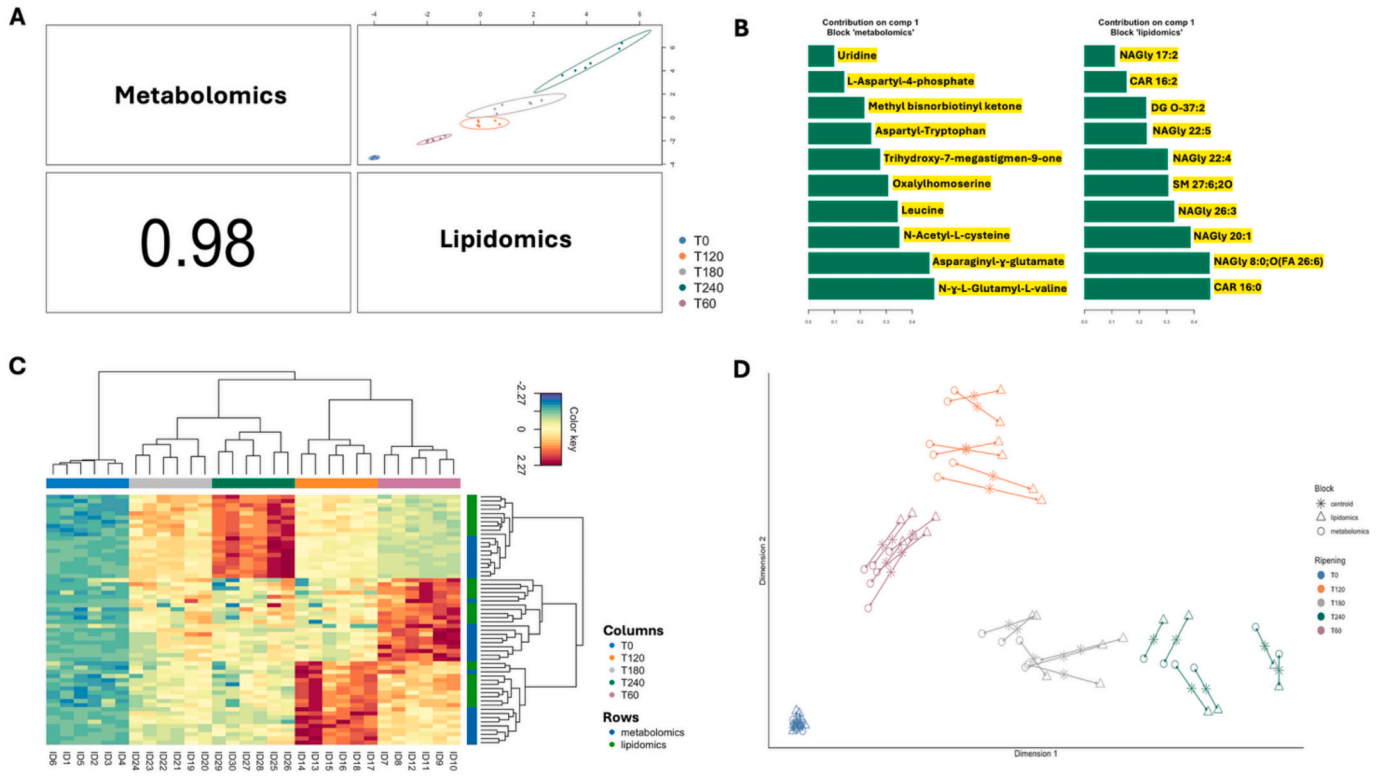


Fig. 1. Multi-omics integration of metabolomic and lipidomic datasets during Pancetta Piacentina PDO ripening using the DIABLO framework (mixOmics). (A) Correlation between the first latent components of the metabolomics and lipidomics blocks ($r = 0.98$), showing the separation of samples according to ripening time (T0–T240). (B) Top ten discriminant metabolites and lipids selected by the DIABLO model as the main contributors to sample separation along the first latent component. (C) Hierarchical clustering heatmap based on the integrated set of variables selected by DIABLO from both omics datasets. For readability, variable names are reported in supplementary Table 5 (sheet k). (D) Arrow plot showing the agreement between metabolomic and lipidomic sample projections across ripening stages.

associated with proteolysis, such as aspartyl-tryptophan (MSI level 3), asparaginyl-gamma-glutamate (MSI level 2), and N-gamma-L-glutamyl-L-valine (MSI level 3). Their accumulation, particularly that of aspartyl-tryptophan ($log_2FC = 11.55$), is consistent with progressive muscle protein degradation during dry-curing (Heres et al., 2023). Also, putative N-gamma-L-glutamyl-L-valine may contribute to sensory development because it has been associated with kokumi taste, with a reported threshold of 550 μmol/kg (Wang et al., 2022). *N*-acetyl-L-cysteine (MSI level 3) further indicated a potential involvement of thiol-related redox pathways (Paulsen & Carroll, 2013), whereas putative trihydroxy-megastigmenone (MSI level 3) was consistent with oxidative degradation. The lipidomic block was characterized by N-acyl glycines, carnitines, diacylglycerols, and sphingomyelins. NAGly 22:5, NAGly 22:4, and NAGly 20:1 increased strongly at T240, while CAR 16:0 and CAR 16:2 may reflect fatty acid mobilization and transport following triglyceride and phospholipid hydrolysis (Longo et al., 2016). SM 27:6;2O further supported membrane lipid remodeling. The hierarchical clustering heatmap and arrow plot (Fig. 1C, D) separated samples according to ripening stage and illustrated the relationships between metabolomic and lipidomic projections. Taken together, the DIABLO analysis identified sets of metabolomic and lipidomic variables that contributed jointly to the discrimination of ripening stages, with the selected features being consistent with proteolytic, lipid-remodeling, and oxidative changes observed during ripening. These associations should nevertheless be interpreted as model-derived relationships rather than as evidence of direct biochemical coordination or causal interactions between the identified molecular features. A limitation is that untargeted metabolomics and lipidomics were performed exclusively in positive electrospray ionization mode. Consequently, compounds preferentially ionizing in negative mode, including several acidic metabolites, oxidized lipids, free fatty acids, and specific phospholipid subclasses, may be underrepresented. The present characterization therefore reflects the molecular fraction detectable under the adopted conditions, while future analyses combining both ionization modes could provide broader metabolome and lipidome coverage.

3.5. *Volatile and sensory profiles of Pancetta Piacentina PDO during ripening*

Descriptive sensory analysis and GC × GC-TQ volatile profiling were evaluated as complementary analytical layers to the biochemical characterization of Pancetta Piacentina PDO ripening (Fig. 2). Sensory analysis showed a progressive transition from fresh pork characteristics toward the profile of a long-ripened dry-cured meat (Fig. 2A). T60 samples showed higher fresh meat aroma and chewiness, whereas prolonged ripening increased meltability and buttery aroma while reducing fresh meat notes. These sensory changes were consistent with the lipid remodeling and structural changes observed by lipidomics and metabolomics, although no formal statistical integration between sensory and omics datasets was performed. The reduction in fresh meat aroma reflects the transition toward the more complex aromatic profile developed during curing (Fu et al., 2022). Rancid aroma became more perceptible at advanced ripening stages but remained moderate, suggesting a contribution of controlled lipid oxidation to aroma complexity (Domínguez, Pateiro, et al., 2019). Slight increases in bitterness and astringency at T240 may be associated with low-molecular-weight peptides, including aspartyl-tryptophan, histidinyl-tryptophan, and thyronine (Supplementary Table 5, sheet d), generated during ripening (Harmon et al., 2024; Kęska & Stadnik, 2017). Volatile profiling identified 59 putatively annotated volatile organic compounds, mainly

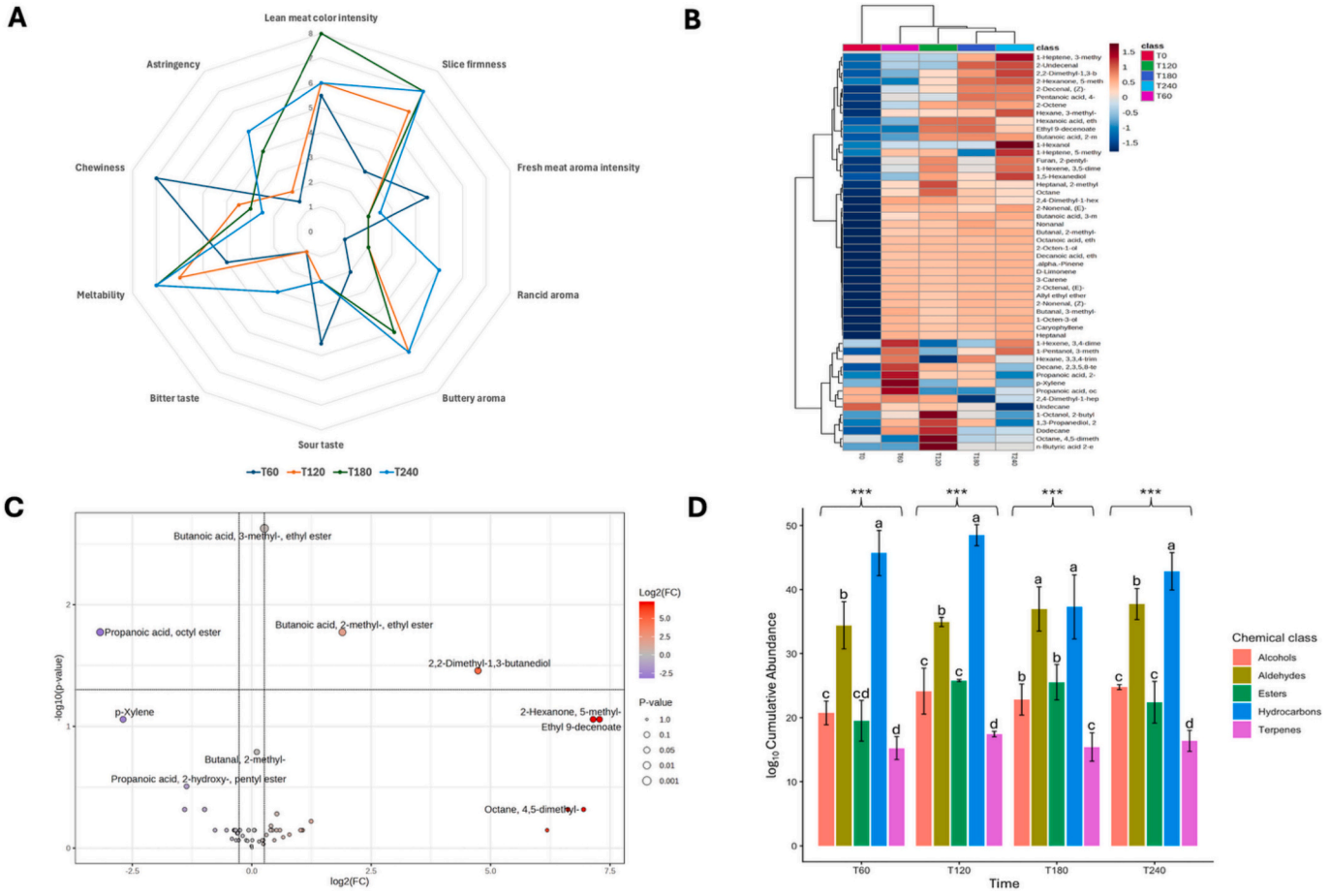


Fig. 2. Sensory and volatile evolution of Pancetta Piacentina PDO during ripening. (A) Radar plot showing the sensory attributes significantly affected by ripening. (B) Hierarchical clustering heatmap of the volatile compounds identified by GC × GC-TQ. (C) Volcano plot comparing short-ripened (T60) and long-ripened (T120, T180, and T240) samples (FDR-adjusted $p < 0.05$; absolute fold change ≥ 1.2). (D) Cumulative $\log_{10}$ abundance index of the main volatile chemical classes during ripening. Values were obtained by summing the $\log_{10}$-transformed abundance values of individual volatile compounds within each chemical class. Different letters within each ripening stage (T60, T120, T180, and T240) indicate significant differences among volatile classes within that ripening stage (*** = $p < 0.001$).

alcohols, aldehydes, esters, hydrocarbons, and terpenes (Supplementary Table 5, sheet l). HCA separated T60 from T120–T240, indicating that the overall volatile fingerprint differed between early and intermediate-to-advanced ripening stages (Fig. 2B). The close clustering of T120, T180, and T240 indicates greater similarity among these later ripening stages, although individual volatile compounds continued to vary. Accordingly, an exploratory comparison between early ripening (T60) and advanced ripening (T120–T240) identified a limited number of discriminant compounds (Fig. 2C). Ethyl 2-methylbutanoate and ethyl 3-methylbutanoate were the most strongly discriminant compounds in the advanced-ripening group. These branched-chain esters have been associated with the catabolism of leucine and isoleucine followed by esterification during meat ripening (Ferrocino et al., 2018), and may contribute to mature and fermented aroma notes (Domínguez, Purrinos, et al., 2019). Conversely, 2-methylbutanal, *p*-xylene, and selected propanoic acid esters were relatively more abundant at T60, although only octyl propanoate was significantly associated with early ripening. The class-level distribution of volatile compounds is shown in Fig. 2D. The cumulative $\log_{10}$ abundance values reported in this panel represent a composite index obtained by summing the $\log_{10}$-transformed abundance values of individual compounds within each chemical class and were used for within-stage comparison among volatile classes. Therefore, these values do not represent total class abundance or absolute concentration and should not be interpreted as evidence of temporal accumulation or depletion of individual volatile classes. Temporal variation was assessed separately by one-way ANOVA for each volatile class. Additionally, hydrocarbons showed significant temporal variation ($p = 0.0223$), whereas no significant temporal variation was detected for alcohols ($p = 0.242$), aldehydes ($p = 0.461$), esters ($p = 0.0611$), or terpenes ($p = 0.404$) (Supplementary Table 5, sheet l). The volatile profile indicates that ripening was associated primarily with changes in individual volatile compounds and in the overall fingerprint, rather than with a uniform shift across volatile chemical classes. These observations are consistent with the changes in PUFA proportions, peroxide value, and TBARS, as well as the lipid remodeling observed by untargeted lipidomics, providing complementary evidence of biochemical transformations during Pancetta Piacentina PDO ripening. Volatile and sensory data were therefore interpreted as complementary evidence alongside, rather than as formally integrated components of, the metabolomics–lipidomics analysis.

4. Conclusions

This study provides a comprehensive multi-platform characterization of the biochemical and sensory evolution of Pancetta Piacentina PDO during ripening, combining compositional, redox, fatty acid, untargeted metabolomic, lipidomic, volatile, and sensory analyses. Ripening was characterized by moisture loss, changes in lipid composition and oxidation markers, extensive metabolic remodeling, proteolysis, and transformations potentially associated with microbial metabolism, collectively contributing to the evolution of product quality. In particular, the reduction in the relative proportion of PUFA,

marked alteration of the endogenous glutathione system, and extensive remodeling of the metabolome and lipidome highlighted redox- and lipid-related changes as important features of maturation. Formal DIABLO analysis of the metabolomics and lipidomics datasets identified model-derived associations between selected molecular features contributing to the discrimination of ripening stages. Volatile and sensory analyses provided complementary evidence of the development of aroma, texture, and flavor characteristics during maturation. Overall, the evolution of Pancetta Piacentina PDO appears to result from the interplay of lipid-related oxidation, proteolysis, and broader metabolic remodeling rather than from changes in individual molecular features alone. The multi-platform analytical strategy adopted in this study provides a comprehensive framework for investigating biochemical and sensory changes during ripening of traditional dry-cured meat products. The molecular features identified here may represent candidates for further investigation as potential indicators of technological maturity, authenticity, or quality, but their potential use as indicators requires validation in independent samples and across different production conditions. Further research should therefore assess the reproducibility and specificity of the observed molecular signatures across different ripening conditions, production batches, and PDO products.

CRediT authorship contribution statement

Gabriele Rocchetti: Writing – review & editing, Writing – original draft, Supervision, Software, Investigation, Formal analysis, Data curation. **Federico Froldi:** Writing – original draft, Investigation. **Giulia Fappani:** Investigation. **Michela Errico:** Investigation, Data curation. **Maria Chiara Fontanella:** Writing – original draft, Investigation. **Samantha Sigolo:** Writing – original draft, Investigation. **Alessandra Scansani:** Investigation, Data curation. **Aldo Prandini:** Writing – review & editing, Supervision, Conceptualization.

Declaration of competing interest

The authors declare that they have no known competing financial interests or personal relationships that could have appeared to influence the work reported in this paper.

Acknowledgements

This work was supported by “Consorzio Salumi DOP Piacentini”, Studio e ricerca impronte indelebili per “Pancetta Piacentina DOP”.

Appendix A. Supplementary data

Supplementary data to this article can be found online at https://doi.org/10.1016/j.foodres.2026.120837.

Data availability

Data are available as Supplementary Table 5

References

Adamsen, C. E., Møller, J. K. S., Laursen, K., Olsen, K., & Skibsted, L. H. (2006). Zn-porphyrin formation in cured meat products: Effect of added salt and nitrite. *Meat Science, 72*(4), 672–679.

AOAC. (1990). *Official methods of analysis* (15th ed.). Arlington: Association of Official Analytical Chemists.

AOAC. (2000). *Official methods of analysis* (17th ed.). Gaithersburg, Md: Association of Official Analytical Chemists.

Aquilano, K., Baldelli, S., & Ciriolo, M. R. (2014). Glutathione: New roles in redox signaling for an old antioxidant. *Frontiers in Pharmacolgy, 5*, 196.

Baldelli, S., Ciccarone, F., Limongi, D., Checconi, P., Palamara, A. T., & Ciriolo, M. R. (2019). Glutathione and nitric oxide: Key team players in use and disuse of skeletal muscle. *Nutrients, 11*(10), 2318.

Breslow, D. K., & Weissman, J. S. (2010). Membranes in balance: Mechanisms of sphingolipid homeostasis. *Molecular Cell, 40*, 267–279.

Busconi, M., Zacconi, C., & Scolari, G. (2014). Bacterial ecology of PDO Coppa and pancetta Piacentina at the end of ripening and after MAP storage of sliced product. *International Journal of Food Microbiology, 172*, 13–20.

Caballero, V., Sánchez-Terrón, G., & Estévez, M. (2025). Metabolomic profiling of Iberian dry-cured ham: Preliminary approach to discriminate between hams from different commercial categories. *Meat Science, 227*, Article 109854.

Castro-Cegrí, A., Ortega-Munoz, M., Sierra, S., Carvajal, F., Santoyo-Gonzalez, F., Garrido, D., & Palma, F. (2023). Application of polysaccharide-based edible coatings to improve the quality of zucchini fruit during postharvest cold storage. *Scientia Horticulturae, 314*, Article 111941.

Christie, W. W. (1989). *Gas chromatography and lipids—A practical guide*. Dundee: The Oily Press.

Colville, L., Blanco Sáez, C. M., Lewis, G. P., & Kranner, I. (2015). The distribution of glutathione and homoglutathione in leaf, root and seed tissue of 73 species across the three sub-families of the Leguminosae. *Phytochemistry, 115*, 175–183.

Commission Regulation (EC) No. 1263/96 of 1 July 1996 supplementing the Annex to the Regulation (EC) No. 1107/96 on the registration of geographical indications and designations of origin under the procedure laid down in Article 17 of Regulation (EEC) No 2081/92.

Domaradzki, P., Nowakowicz-Dębek, B., Wlazło, Ł., Ossowski, M., Dmoch, M., & Florek, M. (2022). Fatty acid composition of muscle and adipose tissue in pigs fed with addition of natural sorbents. *Animals, 12*(13), 1681.

Domínguez, R., Pateiro, M., Gagaoua, M., Barba, F. J., Zhang, W., & Lorenzo, J. M. (2019). A comprehensive review on lipid oxidation in meat and meat products. *Antioxidants, 8*(10), 429.

Domínguez, R., Purrinos, L., Pérez-Santaescolástica, C., Pateiro, M., Barba, F. J., Tomasevic, I., Bastianello Campagnol, P. C., & Lorenzo, J. M. (2019). Characterization of volatile compounds of dry-cured meat products using HS-SPME-GC/MS technique. *Food Analytical Methods, 12*, 1263–1284.

Dragoev, S. G. (2024). Lipid peroxidation in muscle foods: Impact on quality, safety and human health. *Foods, 13*(5), 797.

Dyall, S. C., Balas, L., Bazan, N. G., Brenna, J. T., Chiang, N., et al. (2022). Polyunsaturated fatty acids and fatty acid-derived lipid mediators: Recent advances in the understanding of their biosynthesis, structures, and functions. *Progress in Lipid Research, 86*, Article 101165.

Ferreira, V. C., Martins, T. D., Batista, E. D., Santos, E. P., Silva, F. A., Araujo, I. B., et al. (2013). Physicochemical and microbiological parameters of dried salted pork meat with different sodium chloride levels. *Food Science and Technology, 33*, 382–386.

Ferrocino, I., Bellio, A., Giordano, M., Macori, G., Romano, A., Rantsiou, K., Decastelli, L., & Cocolin, L. (2018). Shotgun metagenomics and volatilome profile of the microbiota of fermented sausages. *Applied and Environmental Microbiology, 84*. e02120–17.

Fu, H., Jin, J., Xiao, S., Wang, J., Li, Y., Li, T., Li, X., Tu, J., Fu, W., Wen, H., Wang, Q., & Wang, M. (2025). The analysis of distinctive lipid metabolism characteristics in dry-cured beef during processing. *Food Chemistry: X, 28*, Article 102540.

Fu, Y., Cao, S., Yang, L., & Li, Z. (2022). Flavor formation based on lipid in meat and meat products: A review. *Journal of Food Biochemistry, 46*, Article e14439.

Ghosh, T., Philtron, D., Zhang, W., Kechris, K., & Ghosh, D. (2021). Reproducibility of mass spectrometry based metabolomics data. *BMC Bioinformatics, 22*, 423.

González-Domínguez, Á., Estanyol-Torres, N., Brunius, C., Landberg, R., & González-Domínguez, R. (2024). QComics: Recommendations and guidelines for robust, easily implementable and reportable quality control of metabolomics data. *Analytical Chemistry, 96*(3), 1064–1072.

Harmon, C. P., Ahmed, O. M., & Breslin, P. A. S. (2024). Amino acid bitterness: Characterization and suppression. *Journal of Agricultural and Food Chemistry, 72*, 22753–22765.

Heres, A., Mora, L., & Toldrá, F. (2023). Bioactive and sensory di- and tripeptides generated during dry-curing of pork meat. *International Journal of Molecular Sciences, 24*(2), 1574.

International Organization for Standardization (ISO). (1973). *Determination of total fat content – Meat and meat products. Method 1443. ISO, Geneva, Switzerland*.

International Organization for Standardization (ISO). (1997). *Determination of moisture content – Meat and meat products. Reference method ISO 1442. ISO, Geneva, Switzerland*.

International Organization for Standardization (ISO). (1998). *Meat and meat products — Determination of total ash. Method 936; ISO: Geneva, Switzerland*.

Jia, S., Shen, H., Wang, D., Liu, S., Ding, Y., & Zhou, X. (2024). Novel NaCl reduction technologies for dry-cured meat products and their mechanisms: A comprehensive review. *Food Chemistry, 431*, Article 137142.

Jin, G., Zhang, J., Yu, X., Zhang, Y., Lei, Y., & Wang, J. (2010). Lipolysis and lipid oxidation in bacon during curing and drying-ripening. *Food Chemistry, 123*(2), 465–471.

Kęska, P., & Stadnik, J. (2017). Taste-active peptides and amino acids of pork meat as components of dry-cured meat products: An in-silico study. *Journal of Sensory Studies, 32*, Article e12301.

Leni, G., Rocchetti, G., Bertuzzi, T., Abate, A., Scansani, A., Froldi, F., & Prandini, A. (2024). Volatile compounds, gamma-glutamyl-peptides and free amino acids as biomarkers of long-ripened protected designation of origin Coppa Piacentina. *Food Chemistry, 440*, Article 138225.

Li, T., He, H., Zhang, E., Hu, F., Wang, Z., Xu, J., Zeng, M., & Peng, B. (2026). The physiological and pathological effects of sphingolipid metabolism and signaling in the central nervous system. *Brain Pathology, 36*(1), Article e70033.

Liang, E., Liu, B., Li, S., Wu, Q., Wang, T., Liu, M., Zhao, Y., Wang, S., & Zhang, S. (2025). Effect of salt on volatile flavor substances in meat products-a review. *LWT, 238*, Article 118857.

Liu, Y., Li, Q., Liu, R., Wang, Z., & Zhao, S. (2026). Exploring the multifunctional roles of betaine: Traditional applications, emerging technologies, and green chemistry innovations. *Foods, 15*(4), Article 737.

Longo, N., Frigeni, M., & Pasquali, M. (2016). Carnitine transport and fatty acid oxidation. *Biochimica et Biophysica Acta (BBA) - molecular Cell Research, 1863*(10), 2322–2435.

Marušić, N., Aristoy, M.-C., & Toldrá, F. (2013). Nutritional pork meat compounds as affected by ham dry-curing. *Meat Science, 93*(1), 53–60.

Mediani, A., Hamezah, H. S., Jam, F. A., Mahadi, N. F., Chan, S. X. Y., Rohani, E. R., Che Lah, N. H., Azlan, U. K., Khairul Annuar, N. A., Azman, N. A. F., Bunawan, H., Sarian, M. N., Kamal, N., & Abas, F. (2022). A comprehensive review of drying meat products and the associated effects and changes. *Frontiers in Nutrition, 9*, 1057366.

Mora, L., Gallego, M., Escudero, E., Reig, M., Aristoy, M.-C., & Toldrà, F. (2015). Small peptides hydrolysis in dry-cured meats. *International Journal of Food Microbiology, 6*, 212–219.

O'Fallon, J. V., Busboom, J. R., Nelson, M. L., & Gaskins, C. T. (2007). A direct method for fatty acid methyl ester synthesis: Application to wet meat tissues, oils, and feedstuffs. *Journal of Animal Science, 85*, 1511–1521.

Pang, Z., Lu, Y., Zhou, G., Hui, F., Xu, L., Viau, C., Spigelman, A. F., MacDonald, P. E., Wishart, D. S., Li, S., & Xia, J. (2024). MetaboAnalyst 6.0: Towards a unified platform for metabolomics data processing, analysis and interpretation. *Nucleic Acids Research, 52*, W398–W406.

Paulsen, C. E., & Carroll, K. S. (2013). Cysteine-mediated redox signaling: Chemistry, biology, and tools for discovery. *Chemical Reviews, 113*(7), 4633–4679.

Petrova, I., Aasen, I. M., Rustad, T., & Eikevik, T. M. (2015). Manufacture of dry-cured ham: A review. Part 1. Biochemical changes during the technological process. *European Food Research and Technology, 241*, 587–599.

Pleadin, J., Lesic, T., Vujacic, V., Milicevic, D., Buneta, A., Susnic, S., Lukanic, I., Kresic, G. (2021). Comparison of chemical composition and fatty acid profile traditional meat products from Croatian and Montenegro. Journal of Food Quality 2021, 5586436.

Reitznerová, A., Šuleková, M., Nagy, J., Marcinčák, S., Semjon, B., Čertík, M., & Klempová, T. (2017). Lipid peroxidation process in meat and meat products: A comparison study of malondialdehyde determination between modified 2-thiobarbituric acid spectrophotometric method and reverse-phase high-performance liquid chromatography. *Molecules, 22*(11), 1988.

Regulation (EU) No 1169/2011 of the European Parliament and of the Council of 25 October 2011 on the provision of food information to consumers, amending Regulations (EC) No 1924/2006 and (EC) No 1925/2006 of the European Parliament and of the Council, and repealing Commission Directive 87/250/EEC, Council Directive 90/496/EEC, Commission Directive 1999/10/EC, Directive 2000/13/EC of the European Parliament and of the Council, Commission Directives 2002/67/EC and 2008/5/EC and Commission Regulation (EC) No 608/2004 (Text with EEA relevance).

Rocchetti, G., Leni, G., Errico, M., Sigolo, S., Lolli, V., Scansani, A., et al. (2025). An integrated approach based on UHPLC-HRMS, ^{1}H-NMR and sensory analysis reveals the exclusive lipid fingerprint of long-ripened protected designation of origin Coppa Piacentina. *Food Chemistry, 469*, Article 142612.

Rocchetti, G., Scansani, A., Leni, G., Sigolo, S., Bertuzzi, T., & Prandini, A. (2023). Untargeted metabolomics combined with sensory analysis to evaluate the chemical changes in Coppa Piacentina PDO during different ripening times. *Molecules, 28*(5), 2223.

Ruiz-Ramírez, J., Arnau, J., Serra, X., & Gou, P. (2005). Relationship between water content, NaCl content, pH and texture parameters in dry-cured muscles. *Meat Science, 70*, 579–587.

Rutigliano, M., Loizzo, P., Spadaccino, G., Trani, A., Tremonte, P., Coppola, R., Dilucia, F., Di Luccia, A., & la Gatta, B. (2023). A proteomic study of "Coppa Piacentina": A typical Italian dry-cured salami. *Food Research International, 166*, Article 112613.

Salek, R. M., Steinbeck, C., Viant, M. R., Goodacre, R., & Dunn, W. B. (2013). The role of reporting standards for metabolite annotation and identification in metabolomic studies. *GigaScience, 2*(1), 13.

Seo, J.-K., Lee, Y. S., Eom, J.-U. K., & Yang, H.-S. (2024). Comparing physicochemical properties, fatty acid profiles, amino acid composition, and volatile compounds in dry-cured loin: The impact of different levels of proteolysis and lipid oxidation. *Food Science of Animal Resources, 44*(1), 103–118.

Seong, P. N., Park, K. M., Kang, G. H., Cho, S. H., Park, B. Y., & Ba, H. V. (2015). The impact of ripening time on technological quality traits, chemical change and sensory characteristics of dry-cured loin. *Asian-Australasian Journal of Animal Sciences, 28*(5), 677–685.

Sha, K., Lang, Y.-M., Sun, B.-Z., Su, H.-W., Li, H.-P., Zhang, L., Lei, Y.-H., Li, H.-B., & Zhang, Y. (2016). Changes in lipid oxidation, fatty acid profile and volatile compounds of traditional Kazakh dry-cured beef during processing and storage. *Journal of Food Processing and Preservation, 41*(4), Article e13059.

Tatiyaborworntham, N., Oz, F., Richards, M. P., & Wu, H. (2022). Paradoxical effects of lipolysis on the lipid oxidation in meat and meat products. *Food Chemistry: X., 14*, Article 100317.

Tomas, M., García-Pérez, P., Rivera-Pérez, A., Patrone, V., Giuberti, G., Lucini, L., & Capanoglu, E. (2024). The addition of polysaccharide gums to *Aronia melanocarpa* purees modulates the bioaccessibility of phenolic compounds and gut microbiota: A multiomics data fusion approach following in vitro digestion and fermentation. *Food Chemistry, 439*, Article 138231.

Tsugawa, H., Cajka, T., Kind, T., et al. (2015). MS-DIAL: Data-independent MS/MS deconvolution for comprehensive metabolome analysis. *Nature Methods, 12*, 523–526.

Vasconcelos, L., Dias, L. G., Leite, A., Lorenzo, J. M., Teixeira, A., Rodrigues, S. S. Q., & Mateo, J. (2025). Dry-cured Bísaro ham: Differences in physicochemical characteristics, fatty acid profile and volatile compounds between muscles. *Foods, 14*(14), 2474.

Wang, H., Suo, R., Liu, X., Wang, Y., Sun, J., Liu, Y., Wang, W., & Wang, J. (2022). Kokumi γ-glutamyl peptides: Some insight into their evaluation and detection, biosynthetic pathways, contribution and changes in food processing. *Food Chemistry Advances, 1*, Article 100061.

Xia, W., & Budge, S. M. (2018). Simultaneous quantification of epoxy and hydroxy fatty acids as oxidation products of triacylglycerols in edible oils. *Journal of Chromatography A, 1537*, 83–90.

Yu, D., & Gu, Y. (2025). Characterization of aroma-active compounds in five dry-cured hams based on electronic nose and GC-MS-olfactometry combined with odor description, intensity, and hedonic assessment. *Foods, 14*, 2305.

Zhang, Q., Chen, B., Ma, P., Yi, L., Gu, Y., & Wang, S. (2026). Emerging insights into lipid oxidation in dry-cured meats: Adverse effects on product quality and safety. *Journal of Future Foods*. https://doi.org/10.1016/j.jfutfo.2026.01.034

Zhao, S., He, L., Zhang, M., Liu, X., & Jin, G. (2020). Effect of salt promote the muscle triglyceride hydrolysis during dry-salting by inducing the phosphorylation of adipose tissue triglyceride lipase (ATGL) and hormone-sensitive lipase (HSL) and lipid droplets splitting. *Food Chemistry, 327*, Article 127061.

Zhu, X., Ma, Z., Zhang, X., Huang, X., Liu, J., & Zhuang, X. (2022). Effect of malondialdehyde-induced oxidation modification on physicochemical changes and gel characteristics of duck myofibrillar proteins. *Gels, 8*, 633.